OPTICA

High-sensitivity frequency comb carrier-envelope-phase metrology in solid state high harmonic generation

Daniel M. B. Lesko,[1,2,3,*] Kristina F. Chang,[1] and Scott A. Diddams[1,3,4,5]

[1]Time and Frequency Division, National Institute of Standards and Technology, Boulder, Colorado 80305, USA
[2]Department of Chemistry, University of Colorado Boulder, Colorado 80309, USA
[3]Department of Physics, University of Colorado Boulder, Colorado 80309, USA
[4]Department of Electrical, Computer and Energy Engineering, University of Colorado, Boulder, Colorado 80309, USA
[5]e-mail: Scott.Diddams@colorado.edu
*Corresponding author: Daniel.Lesko@colorado.edu

Received 7 June 2022; revised 16 September 2022; accepted 20 September 2022; published 19 October 2022

Non-perturbative and phase-sensitive light–matter interactions have led to the generation of attosecond pulses of light and the control of electrical currents on the same time scale. Traditionally, probing these effects via high harmonic generation has involved complicated lasers and apparatuses to generate the few-cycle and high peak power pulses needed to obtain and measure spectra that are sensitive to the phase of the light wave. Instead, we show that nonlinear effects dependent on the carrier-envelope phase can be accessed in solid state crystals with simple, low pulse energy frequency combs that we combine with high-sensitivity demodulation techniques to measure harmonic spectral modulations. Central to this advance is the use of a scalable 100 MHz erbium-fiber frequency comb at 1550 nm to produce 12 nJ, 20 fs pulses that are focused to the TW/cm^2 level. In a single pass through a 500 μm ZnO crystal, this yields harmonic spectra extending down to 200 nm. With this system, we introduce a technique of carrier-envelope amplitude modulation spectroscopy (CAMS) and use it to characterize the phase-sensitive modulation of the ultraviolet harmonics with an 85 dB signal-to-noise ratio. We further verify the non-perturbative nature of the harmonic generation through polarization gating of the driving pulse to increase the effects of the carrier-envelope phase. This work demonstrates robust and ultra-sensitive methods for generating and characterizing harmonic generation at 100 MHz rates that should provide advantages in the study of attosecond nonlinear processes in solid state systems. Additionally, as a simple and low-noise frequency comb, this broadband source will be useful for precision dual-comb spectroscopy of a range of physical systems across the ultraviolet and visible spectral regions (200–650 nm).

https://doi.org/10.1364/OPTICA.465709

1. INTRODUCTION

Non-perturbative and phase-sensitive nonlinear optics opens new windows to physical phenomena in gases, liquids, and solids on the attosecond time scale [1]. These attosecond (10^{-18} s) processes in atomic [2–4] and solid state semiconductor systems [5–11] are most commonly probed by way of light emitted from high harmonic generation (HHG). Conductors, low-bandgap semiconductors, and plasmonics [12–23] similarly exhibit these attosecond phenomena but are probed by phase-sensitive current generation. Such ultrafast physical phenomena in both high and low-bandgap materials can potentially be used for generating and controlling ultrafast transient currents for petahertz (10^{18} Hz) electronics and exploring light–matter interactions at attosecond time scales [1,12,21,22,24–26]. Despite the large energy difference in optical fields required to drive these processes, the requirement of stable few-cycle optical pulses for exciting subcycle dynamics is common across this wide range of research topics. Probing these dynamics require pulses with a well-defined carrier-envelope phase (CEP), i.e., a repeatable and controllable waveform, to provide a known electric potential on the time scale of the cycle of light.

Non-perturbative HHG processes in gases and semiconductors typically require high-power lasers with μJ to mJ energies and ≤10 kHz repetition rates. But similar phase-dependent processes are present in solid state conductors (and low-bandgap semiconductors), which require significantly lower optical energies, in the nJ range, and are, therefore, compatible with pulsed sources in the 100 MHz range. To elucidate the phase sensitivity in the HHG process, the CEP is locked to a well-defined value and slowly scanned to measure the phase-dependent spectral shifts [2–4,6–11,27]. This technique relies on the high fluxes achieved with low repetition rate sources to produce measurable spectral shifts with a grating spectrometer. On the other hand, when exploring these processes in low-bandgap (or zero-bandgap) materials, one can take advantage of the high repetition rate and high frequency

modulation and demodulation techniques to perform similar measurements [12,15]. With a nonzero f_{ceo}, the CEP cycles through 2π at a well-defined rate. By using lock-in detection at f_{ceo}, and simple symmetry arguments, one can determine the phase-dependent current generation as well as the contributions of the interband and intraband currents to the total signal [12]. However, this approach measures a different observable (electronic currents) and uses lasers that lack the required flux to measure CEP-dependent HHG. Addressing subcycle attosecond dynamics in HHG with high sensitivity requires a significant advancement in the methods used to detect these CEP-dependent signals.

Here we introduce high-sensitivity frequency comb techniques to study phase-sensitive harmonic generation from solid dielectrics with low energy (nJ) pulses at 100 MHz. This advance is enabled by our technique of low-noise and scalable short pulse generation that overcomes conventionally limited powers from 100 MHz Er:fiber combs to produce 12 nJ 20 fs pulses at 1550 nm [28]. We focus these pulses into 500 μm ZnO (a plane, Miller Index: 11-20) to 2 TW/cm^2, producing harmonics in a near continuum to wavelengths as short as 200 nm, without the need for high pressure hollow core fibers, pulse picking, or complicated vacuum apparatuses. To measure CEP-dependent spectral modulations, we leverage the low-noise properties of our Er:fiber comb to characterize extremely small amplitude modulation sidebands in the ultraviolet (UV) harmonics that arise from the nonzero f_{ceo}. This approach, which we call carrier-envelope amplitude modulation spectroscopy (CAMS), provides 85 dB of signal-to-noise ratio (SNR) at a 1 Hz resolution bandwidth (RBW), allowing us to measure the effect of the CEP cycling in a four-cycle pulse. Analyzing multiple harmonics with CAMS reveals the impact of the crystalline symmetry on the periodic spectral modulations that arise from the pump CEP. We further confirm the non-perturbative nature of our generated light by gating our pulse, effectively shortening it, and observing increased modulation and non-perturbative power scaling. The use of a solid state target and a fiber laser system results in a simple, robust, and vacuum-free apparatus to measure these strong field effects. We anticipate systems like this will be useful not only for measuring field sensitive physics in solids and potentially gases but also for broadband spectroscopy in a dual-comb modality.

2. EXPERIMENTAL SETUP

An outline of the experimental setup is shown in Fig. 1(a). The setup is based on a commercial, 100 MHz low-noise polarization maintaining (PM) Er:fiber oscillator at 1550 nm (Menlo Systems). The f_{ceo} of the oscillator is stabilized by a conventional $f-2f$ interferometer to a maser referenced signal at $f_{ceo}=1$ MHz. This provides a well-defined cycling of the CEP with the sampling defined by $(2\pi f_{ceo})/(f_{rep}) \sim 63$ mrad/pulse for the 100 MHz oscillator. The f_{rep} is not locked but maintains enough stability over a typical 10 s average to negligibly impact the rate of CEP cycling.

The oscillator pulses are amplified and spectrally broadened to support few cycle pulses, as described in [28]. Briefly, the oscillator output is stretched in a normal dispersion fiber and amplified to 20 nJ in a purpose-built erbium/ytterbium-doped fiber amplifier. The pulses are then compressed with a grating compressor, spectrally broadened in PM normal dispersion highly nonlinear fiber (ND-HNLF), and compressed again using fused silica (FS) and third-order dispersion mirrors. The dispersion is optimized

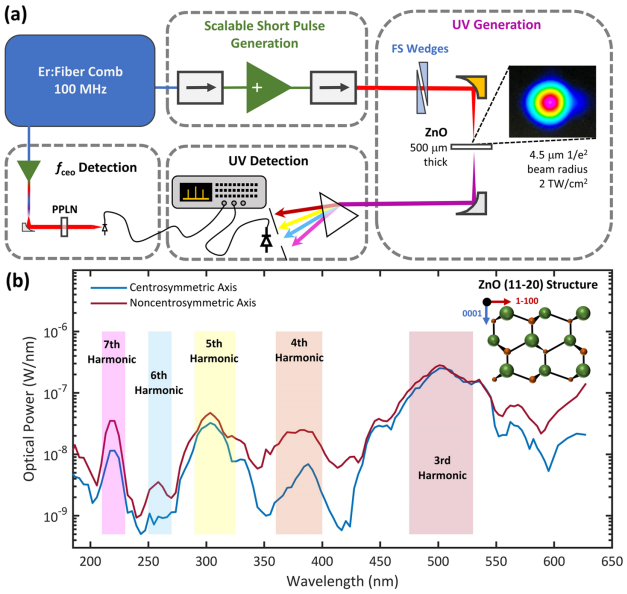

Fig. 1. Overview of solid state high harmonic generation (HHG) driven by a frequency comb: (a) experimental setup utilizing short pulse generation at 1550 nm with a low-noise Er:fiber comb to produce high-power, 20 fs pulses. The pulses drive HHG in a 500 μm thick, a-plane cut ZnO (11-20). Generated UV and visible light is detected by a monochromator and photomultiplier tube. (b) Spectra resulting from HHG in ZnO. HHG oriented along the centrosymmetric axis (0001, blue) yields predominately odd harmonics while the noncentrosymmetic axis (1-100, red) yields both even and odd harmonics. The peak at ~385 nm appears to be consistent with photoluminescence on the centrosymmetric axis demonstrated in [29,30]. Upper right, crystallographic orientation of 11-20 ZnO adapted from [40]. Zinc atoms are depicted in green with oxygen in orange, with relative sizes showing in-page and out-of-page orientation.

with the FS wedges to provide 12 nJ, 20 fs (four-cycle) pulses at the back face of a 500 μm thick a-plane single crystal ZnO (hexagonal wurtzite structure, Miller Index: 11-20). We verify this by second-harmonic generation frequency resolved gating (SHG-FROG, Fig. 1 in Supplement 1), which indicates that linear compression in the ZnO dominates over nonlinear compression processes. Spatially, the pulses are tightly and achromatically focused by an off-axis parabolic mirror (OAP) to a $1/e^2$ radius of 4.5 μm. Placing this focus at the back face of the ZnO minimizes reabsorption of light generated above the ZnO bandgap. The peak power is estimated to be ~0.675 MW corresponding to a peak intensity of >2 TW/cm^2. While the peak power of the pulse is enough to consider self-focusing, the lack of observed self-collapse and spectral broadening for the driving pulse suggests this is not a dominant process for producing high intensities. The dynamics between self-focusing and non-perturbative harmonic generation would be a topic for future study.

The UV and visible (UV/Vis, 200–650 nm) light generated with the ZnO crystal is collected by an OAP with high reflectance in the UV (Acton #1200, 120–600 nm) and sent to a purpose-built monochromator. Our monochromator is based on a 1800 g/mm grating blazed for 250 nm (Richardson Gratings) mounted on a rotation stage and a fast, UV-sensitive photomultiplier tube (PMT, H6780-03 Hamamatsu). The estimated resolving power is $\lambda/\delta\lambda = 125$ at 250 nm. The DC photocurrent produced by the PMT is amplified using a low-noise current pre-amplifier (Femto) and measured simultaneously on an oscilloscope and spectrum

analyzer. At each grating position, the dark photocurrent is measured and subtracted, while the f_{ceo} power is normalized to the f_{rep} power. The power spectral density is calibrated by measuring the third-harmonic yield with a notch filter and powermeter. Due to detector saturation, the spectra of the third and fourth harmonic are taken with a neutral density filter in line before being scaled to match the optical power measured and concatenated with the higher harmonics. A UV Glan–Thompson polarizer is used in a rotation mount to measure the polarization of the generated light.

3. RESULTS

Spectra of UV and visible light from 200–650 nm generated in the ZnO crystal are presented in Fig. 1(b). The cut of the ZnO crystal (a-plane, 11-20) enables the crystal to be oriented such that excitation from the linearly polarized pump pulse primarily occurs along either the centrosymmetric axis (0001, blue) or the noncentrosymmetric axis (1-100, red). Due to crystal symmetry, generation along the centrosymmetric axis predominantly yields odd harmonics of the fundamental 1550 nm driving laser, as well as photoluminescence at ∼385 nm [29,30]. Some even harmonics are also observed along the centrosymmetric axis but are significantly weaker relative to the odd harmonics. The observation of weak even harmonics may arise from harmonic generation at the crystal surface where the symmetry of the crystal is broken, from off-axis generation due the tight focus of the driving laser, or from co-propagating surface generated second harmonic. In contrast, generation along the noncentrosymmetric axis yields both even and odd harmonics, resulting in more continuous spectral coverage compared to the centrosymmetric axis. In both crystal orientations, generation up to the seventh harmonic (∼221 nm) is observed. Given the intensity of the driving pulse, harmonics beyond the 7th harmonic are expected [31,32] but lie beyond the wavelength range of the detector. In both crystal orientations, the harmonics are observed to be primarily co-polarized from the driving laser field. The observation of co-polarized harmonics is consistent with previous HHG experiments in ZnO [33,34]. With the 12 nJ, 100 MHz, driving laser, $>10^{10}$ photons/second/nm are produced at 221 nm, the highest observed harmonic (see Supplement 1, Fig. 2).

With a peak intensity of $>2\,\mathrm{TW/cm^2}$, non-perturbative nonlinear optics should dominate the generation of harmonics [33]. We observe CEP-dependent spectra with a short and tightly focused driving pulse, similar to systems with higher pulse energies and lower repetition rates. To detect and measure these effects, we spectrally filter the generated light using a monochromator and detect the RF spectrum with a high bandwidth UV-sensitive PMT [Fig. 1(a)]. The physical mechanism for non-perturbative HHG in a solid semiconductor can be approximated as a three-step process [8]. In the first step, the electric field of the driving pulse induces the tunneling (interband polarization) of an electron from the valence to the conduction band, leaving a hole in the valence band. In the second step, the electron and its associated hole propagate within the conduction and valence bands, respectively (intraband current). In the third step, the emission of a high-energy photon occurs when the electron and hole pair recombine (interband recombination) or when they generate an intraband current (intraband recombination). The three-step process occurs within a half-cycle of a driving pulse, resulting in the photon emission at half-cycle periodicity and an associated emission spectrum comprised of discrete harmonics. For centrosymmetric solids, the harmonics are comprised of only odd harmonics, whereas noncentrosymmetric solids yield both even and odd harmonics. As the CEP of a few-cycle laser evolves [with an $f_{ceo} \neq 0$, top of Fig. 2(a)] the peak field (potential) of each pulse changes. Each half-cycle of the driving laser produces a UV pulse (bottom) whose amplitude (and spectrum) are dependent on the magnitude of the driving field. As the CEP cycles (left to right), the UV pulses change. The change in the CEP is, thus, imprinted onto the spectrum [Fig. 2(b)(i)] and measured in the time domain as amplitude modulations on the repetition rate of the comb [Fig. 2(b)(ii)]. The Fourier transformation of the monochromator signal [Fig. 2(b)(iii)] reveals the amplitude modulation depth (β) and frequency, which is proportional to the rate at which the CEP cycles (i.e., f_{ceo}). This method of CAMS allows for narrow RBW (1 Hz) to measure modulations as small as −85 dBc, relative the f_{rep} tone, as shown Fig. 2(c). Notably, we only observe f_{ceo} and 2 f_{ceo} in the RF spectra, corresponding to the periodic dependence (2π and π, respectively) of the UV light on the CEP. The effect of the CEP periodicity is seen in Fig. 2(d). When the noncentrosymmetric axis is used, the f_{ceo} tone is significantly increased. This is due to the lack of degeneracy between a CEP of 0 and π (i.e., a cosine and -cosine pulse) in the noncentrosymmetric material. UV generation on the centrosymmetric axis results in a suppression of the f_{ceo} tone. The f_{ceo} does not disappear due to the small amount of surface generated second harmonic [10,35] and tight focusing. Both of these effects slightly break the degeneracy of the two CEP values (0 and π) resulting in f_{ceo} being present on both axes.

Narrowband RF detection allows the possibility for two additional measurements that can be taken. With a lock-in detection scheme, the phase difference between the amplitude modulations at f_{ceo} and $2f_{ceo}$ can be measured as a function of wavelength (Supplement 1, Fig. 3). This measurement could potentially be used to give information on the chirp of the UV pulses, similar to a traditional CEP scan using a grating spectrometer [9]. In future experiments, without spectral filtering by a grating monochrometer, one could observe the center of mass shifts (timing jitter) of the UV pulses relative to the driving laser envelope. The center of mass shift could yield information about the phase delay of the generated UV light with respect to the driving laser's CEP. Here, the analysis at higher harmonics of the f_{rep} could be beneficial, where the timing jitter has a stronger impact on the signal than the amplitude modulation.

With CAMS, we measure the modulation depth β across the spectrum (from 200 nm to 700 nm) for both the centrosymmetric [Fig. 3(a)] and noncentrosymmetric [Fig. 3(b)] axes. As noted above, the increased symmetry breaking on the noncentrosymmetric axis gives much larger β across the spectrum corresponding to increased modulation with a 2π periodicity. On both crystallographic axes, the lower order harmonic's modulation depth follows a trend of being more prominent at the wings of each harmonic and sharply diminished at the center. This is because, at a ∼3.9 cycle pulse length, the positions of the harmonic centers are (i) not shifting dramatically with change of CEP and (ii) being averaged over the entire 2π of the CEP by our integration time (set by the f_{ceo} and RBW). An interesting observation is the flat modulation depth between the 5th and 7th harmonic on the centrosymmetric axis, where only 1 f_{ceo} is present, despite there being no distinguishable 6th harmonic in the spectrum. One would also expect to see $2f_{ceo}$ between these harmonics from heterodyne gain (a $5f - 7f$ interference) if this was a perturbative process. Furthermore, we do not observe any f_{ceo} tone anywhere on the 1550 nm fundamental, which would originate from a cascaded $\chi^{(2)}$ (perturbative) process.

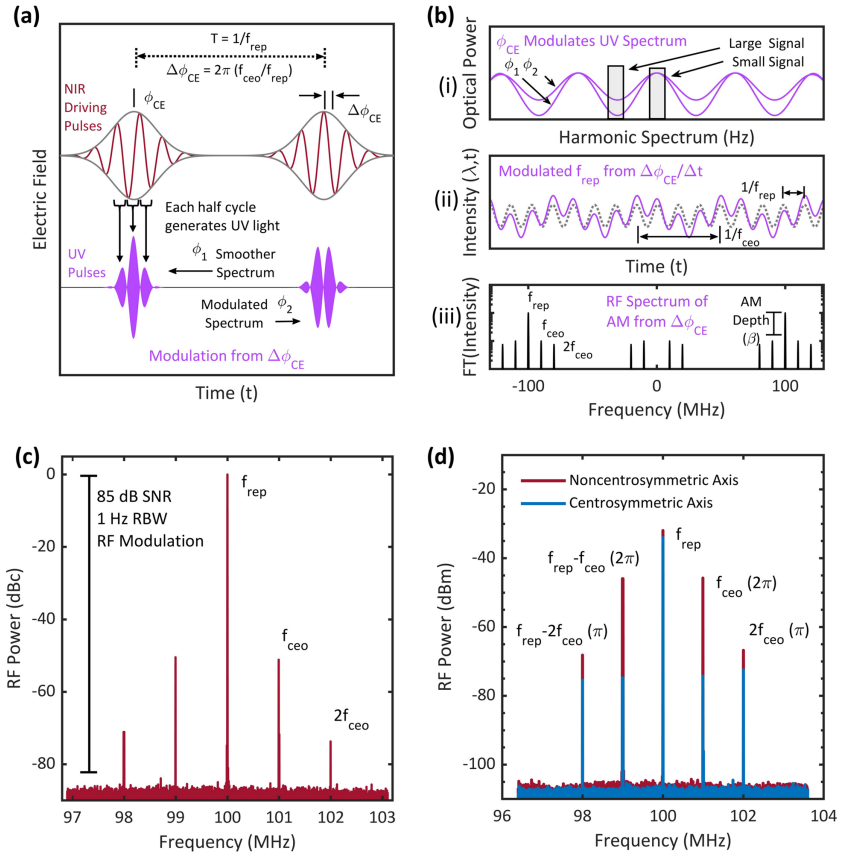

Fig. 2. Amplitude modulation from carrier envelop phase (CEP)-dependent harmonic generation measured by carrier-envelope amplitude modulation spectroscopy (CAMS). (a) Schematic describing the timing of the driving laser pulses with CEP cycling, as well as the resulting CEP-dependent UV generation. Each half-cycle of the driving laser (top) produces a UV pulse (bottom) whose amplitude (and spectrum) is dependent on the magnitude of the driving field. As the CEP evolves (from the left to the right pulse), the generated UV pulse train changes. This difference in UV pulses is imparted onto the generated spectrum. (b) Schematic describing the detection method of the CEP-dependent spectrum. (i) The CEP's dependence can be seen across the spectra, with certain regions yielding larger signals. (ii) Isolating one wavelength region, this CEP-dependent spectral intensity can be seen as modulation on the f_{rep} tone. (iii) A Fourier transform reveals the modulation depth of the CEP-dependent intensity (β) as well as the frequency as well as the CEP cycling frequency (f_{ceo}). (c) At the center of harmonics (data from the third harmonic, ~500 nm), we achieve >85 dB sensitivity to CEP effects allowing for measurements of small modulations. We observe f_{ceo} and 2 f_{ceo} tones in the spectrum. (d) RF spectra at 439 nm showing the effect of symmetry breaking on the relative amplitudes of f_{ceo} and $2f_{ceo}$. The presence of f_{ceo} and $2f_{ceo}$ corresponds to a 2π and π periodicity of the signal on the CEP, respectively.

To further investigate the non-perturbative processes generating the UV/Vis light, we use polarization assisted amplitude gating (PASSAGE) [36] [Fig. 4(a)] to reduce the number of cycles that contribute to the nonlinear process. To implement PASSAGE, two achromatic $\lambda/2$ wave plates impart a λ delay, while an achromatic $\lambda/4$ wave plate imparts ellipticity. We compensate the additional dispersion of the wave plates by adding/removing UVFS glass. The time-varying polarization effectively reduces the number of cycles contributing to the generation of UV light. The impact of such polarization gating has been observed with gases, which exhibit a strong dependence on polarization [36]. However, solids such as MgO and ZnO exhibit anisotropy, and similar polarization-dependent effects on harmonic generation are also expected [30,33,34]. When we measure the modulation depth β as a function of the $\lambda/4$ plate angle, we see an increase of 23.3 dB at 45 deg [Fig. 4(b)]. Furthermore, the shape of the curve and singular peak of the ellipticity on the modulation depth [Fig. 4(b)] suggest that a time-dependent elliptical profile on the driving pulse is largely maintained, despite the birefringence of the a-cut ZnO crystal [30,34]. We model the time-varying ellipticity of the pump pulse, and the effect of the ZnO birefringence is presented in Supplement 1. Since the efficiency of HHG in ZnO, and most solids in general, possesses weaker sensitivity to the polarization [30,34] of the driving pulse than gas phase HHG, the shape of the modulation depth as a function of ellipticity is present but not sharp. Nonetheless, our measurements show that PASSAGE, and more generally polarization gating, can still be applied to solid state HHG in ZnO, yielding an increased sensitivity to the driving laser CEP. The overall yield of UV light is decreased by approximately a factor of 8, which is in agreement to scaling seen in the gas [36] and consistent with a non-perturbative picture. In a perturbative picture, the fifth harmonic light would be reduced by a factor of >10,000 based on a simple I^5 scaling with intensity and the reduction of the driving pulse. This would be far below our detection range.

These arguments are further supported by measurements of the change in modulation depth ($\Delta\beta$) from PASSAGE across part of the UV spectrum [Fig. 4(c)]. If the generation of UV light was governed by perturbative nonlinear optics, we would expect the harmonics to increase in width due to the effectively shorter (subcycle) driving pulse. The $\Delta\beta$, normalized heterodyne gain from $nf-(n-1)f$ interference, from this spectral widening

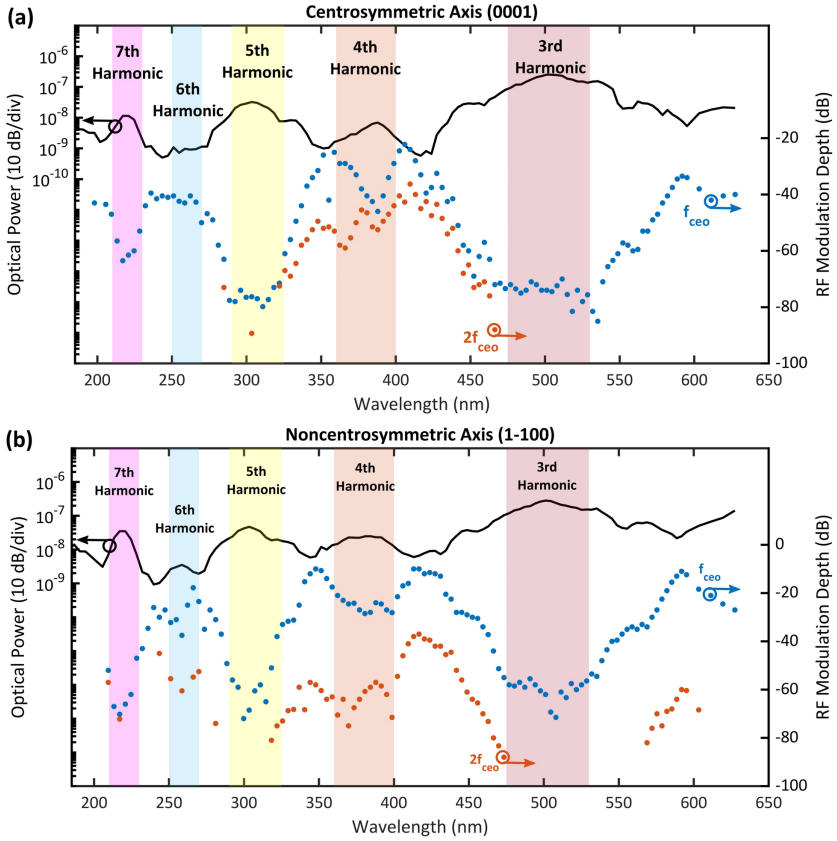

Fig. 3. CAMS spectra of measured RF power modulation (shown as $n f_{ceo}/f_{rep}$) across the UV/Vis spectrum on the (a) centrosymmetric and (b) noncentrosymmetric axes.

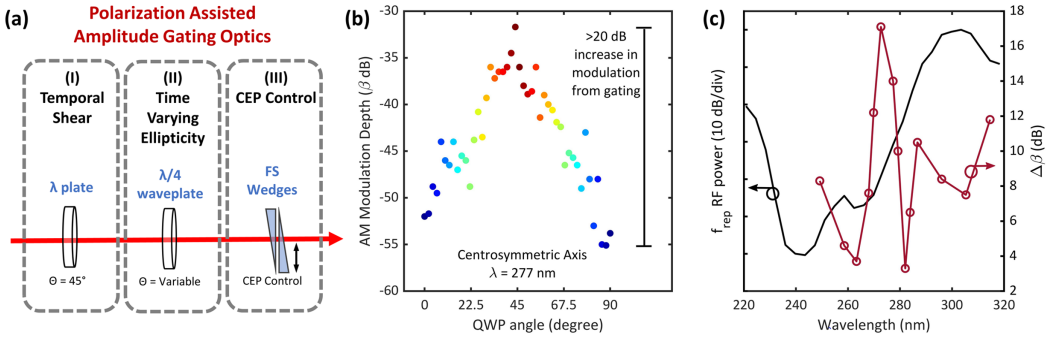

Fig. 4. Increasing the carrier-envelope phase effects in ZnO. (a) We utilize polarization assisted amplitude gating (PASSAGE) to reduce the number of cycles contributing to UV generation. By introducing a (I) temporal shear by a λ plate, we are able to impart a time-dependent ellipticity (II) by a λ/4 plate. This reduces the effective driving pulse to $a < 1$ cycle pulse. Finally we can optimize the CEP and chirp by FS wedges (III). (b) Modulation depth (β) as a function of the λ/4 (QWP, quarter-wave plate) angle, showing a 23.5 dB increase in the UV modulation depth when fewer cycles are used in the generation process. (c) Measured increase in modulation ($\Delta\beta$) from using PASSAGE on the centrosymmetric axis between the seventh and fifth harmonics. The shape of the increase in modulation does not match a perturbative picture of widening harmonics.

would correspond to a increase in signal closer to the center of each harmonic. This would arise from the increase in spectral overlap closer to the center of the harmonics. However, this trend in $\Delta\beta$ is not observed between the fifth and seventh harmonics [Fig. 4(c)]. Deviation in the observed $\Delta\beta$ trend from that expected for a purely perturbative harmonic generation mechanism provides further evidence for a non-perturbative generation mechanism.

The exceptional sensitivity afforded by CAMS exceeds that of a traditional UV spectrometer based on commercially available cameras [37] by several orders of magnitude. Leveraging this high sensitivity, one can envision extending the technique to study the CEP-dependent process in semiconductors, where the CEP-dependent signal would be drastically smaller for the intraband currents than the interband currents [9]. Furthermore, one could probe materials that are thought to not have CEP sensitivity in their interband or intraband currents [38]. These intraband and interband current phenomena have been studied in conductor systems [12] with similar lock-in techniques, but they have not been studied with such sensitivity in semiconductor solids and gases.

While the results in this paper, particularly from the PASSAGE experiments, suggest that the spectrum itself is modulated from

few-cycle, non-perturbative harmonic generation, our detection method is not directly capable of discerning the contributions of amplitude modulation from the CEP-dependent spectrum versus interference between spectrally overlapped harmonics to the overall modulation signal. Fundamentally, the modulation generated from this harmonic interference is insensitive to the absolute CEP of the driving laser, while in a few-cycle and non-perturbative limit, the spectrum itself would shift and modulate with the CEP. Underpinning the picture of harmonic spectral interference is the idea that each comb tooth can be described by the equation $f_{\text{optical}} = q(\text{n}f_{\text{rep}} \pm f_{\text{ceo}})$, where q is the harmonic order and n is the comb tooth number. Interference from spectral overlap between harmonics $q = 5$ and $q = 6$ would result in a f_{ceo} tone and interference between $q = 5$ and $q = 7$ in a $2f_{\text{ceo}}$ tone. While previous experiments (such as Benko *et al*. [39]) succinctly and accurately describe dual extreme UV comb interference with this simple frequency domain equation, it is interesting to question if this basis holds in the high peak field and single-cycle pulse limit.

4. CONCLUSION

In summary, we present a non-perturbative single pass solid state HHG setup based on a robust, low-noise, and compact 100 MHz Er:fiber frequency comb. We utilize high frequency modulation/demodulation techniques to measure the spectral modulation from the CEP cycling with 85 dB SNR. This allows us to measure the spectral modulations across the UV/Vis spectrum from CEP sensitive HHG with a four-cycle pulse. This simple, robust, high intensity, and high repetition rate source will be useful for investigating field-sensitive physics in semiconductor solids and gases that benefit from detection of weak signals and the intrinsic fast averaging at the 100 MHz rate. Furthermore, the broadband UV/Vis spectrum that is generated with the noncentrosymmetric axis of ZnO will match broadband atmospheric UV absorbers such as NO_2 and SO_2 for dual-comb spectroscopy [41, 42]. With the amount of light generated at the fifth harmonic, we estimate it will be possible to measure spectra across 100 THz of optical bandwidth with 10 GHz resolution for averaging times <1 h. Work toward such experiments, including the construction of a second frequency comb system, is ongoing.

Funding. U.S. Air Force (FA9550-16-1-0016, FA9550-22-1-0483); Defense Advanced Research Projects Agency (SCOUT); National Institute of Standards and Technology (70NANB18H006).

Acknowledgment. Mention of specific products or trade names is for technical and scientific information and does not constitute an endorsement by NIST. D. M. B. L. acknowledges award 70NANB18H006 from NIST. K. F. C. acknowledges support from the National Research Council. The authors thank J. Ye and C. Zhang for loaning VUV optics, as well as T. Allison, J. Biegert, M. Chini, S. Ghimire, and F. Quinlan for valuable comments and discussion.

Disclosures. The authors declare no conflicts of interest.

Data availability. Data underlying the results presented in this paper are not publicly available at this time but may be obtained from the authors upon reasonable request.

Supplemental document. See Supplement 1 for supporting content.

REFERENCES

1. F. Krausz and M. I. Stockman, "Attosecond metrology: from electron capture to future signal processing," Nat. Photonics **8**, 205–213 (2014).
2. M. Hentschel, R. Kienberger, C. Spielmann, G. A. Reider, N. Milosevic, T. Brabec, P. Corkum, U. Heinzmann, M. Drescher, and F. Krausz, "Attosecond metrology," Nature **414**, 509–513 (2001).
3. G. Sansone, L. Poletto, and M. Nisoli, "High-energy attosecond light sources," Nat. Photonics **5**, 655–663 (2011).
4. M. Chini, K. Zhao, and Z. Chang, "The generation, characterization and applications of broadband isolated attosecond pulses," Nat. Photonics **8**, 178–186 (2014).
5. M. Garg, M. Zhan, T. T. Luu, H. Lakhotia, T. Klostermann, A. Guggenmos, and E. Goulielmakis, "Multi-petahertz electronic metrology," Nature **538**, 359–363 (2016).
6. S. Ghimire, G. Ndabashimiye, A. D. DiChiara, E. Sistrunk, M. I. Stockman, P. Agostini, L. F. DiMauro, and D. A. Reis, "Strong-field and attosecond physics in solids," J. Phys. B **47**, 204030 (2014).
7. S. Sederberg, D. Zimin, S. Keiber, F. Siegrist, M. S. Wismer, V. S. Yakovlev, I. Floss, C. Lemell, J. Burgdörfer, M. Schultze, F. Krausz, and N. Karpowicz, "Attosecond optoelectronic field measurement in solids," Nat. Commun. **11**, 430 (2020).
8. S. Ghimire and D. A. Reis, "High-harmonic generation from solids," Nat. Phys. **15**, 10–16 (2019).
9. Y. S. You, M. Wu, Y. Yin, A. Chew, X. Ren, S. Gholam-Mirzaei, D. A. Browne, M. Chini, Z. Chang, K. J. Schafer, M. B. Gaarde, and S. Ghimire, "Laser waveform control of extreme ultraviolet high harmonics from solids," Opt. Lett. **42**, 1816–1819 (2017).
10. J. Li, J. Lu, A. Chew, S. Han, J. Li, Y. Wu, H. Wang, S. Ghimire, and Z. Chang, "Attosecond science based on high harmonic generation from gases and solids," Nat. Commun. **11**, 2748 (2020).
11. T. Higuchi, M. I. Stockman, and P. Hommelhoff, "Strong-field perspective on high-harmonic radiation from bulk solids," Phys. Rev. Lett. **113**, 213901 (2014).
12. T. Boolakee, C. Heide, A. Garzón-Ramírez, H. B. Weber, I. Franco, and P. Hommelhoff, "Light-field control of real and virtual charge carriers," Nature **605**, 251–255 (2022).
13. M. R. Bionta, F. Ritzkowsky, M. Turchetti, Y. Yang, D. Cattozzo Mor, W. P. Putnam, F. X. Kärtner, K. K. Berggren, and P. D. Keathley, "On-chip sampling of optical fields with attosecond resolution," Nat. Photonics **15**, 456–460 (2021).
14. P. Hommelhoff, Y. Sortais, A. Aghajani-Talesh, and M. A. Kasevich, "Field emission tip as a nanometer source of free electron femtosecond pulses," Phys. Rev. Lett. **96**, 077401 (2006).
15. W. P. Putnam, R. G. Hobbs, P. D. Keathley, K. K. Berggren, and F. X. Kärtner, "Optical-field-controlled photoemission from plasmonic nanoparticles," Nat. Phys. **13**, 335–339 (2017).
16. B. Piglosiewicz, S. Schmidt, D. J. Park, J. Vogelsang, P. Groß, C. Manzoni, P. Farinello, G. Cerullo, and C. Lienau, "Carrier-envelope phase effects on the strong-field photoemission of electrons from metallic nanostructures," Nat. Photonics **8**, 37–42 (2014).
17. D. J. Park, B. Piglosiewicz, S. Schmidt, H. Kollmann, M. Mascheck, and C. Lienau, "Strong field acceleration and steering of ultrafast electron pulses from a sharp metallic nanotip," Phys. Rev. Lett. **109**, 244803 (2012).
18. C. Heide, M. Hauck, T. Higuchi, J. Ristein, L. Ley, H. B. Weber, and P. Hommelhoff, "Attosecond-fast internal photoemission," Nat. Photonics **14**, 219–222 (2020).
19. M. Krüger, M. Schenk, and P. Hommelhoff, "Attosecond control of electrons emitted from a nanoscale metal tip," Nature **475**, 78–81 (2011).
20. C. Lemell, X.-M. Tong, F. Krausz, and J. Burgdörfer, "Electron emission from metal surfaces by ultrashort pulses: determination of the carrier-envelope phase," Phys. Rev. Lett. **90**, 076403 (2003).
21. C. Schoenfeld, P. Sulzer, D. Brida, A. Leitenstorfer, and T. Kurihara, "Passively phase-locked Er:fiber source of single-cycle pulses in the near infrared with electro-optic timing modulation for field-resolved electron control," Opt. Lett. **47**, 3552–3555 (2022).
22. T. Rybka, M. Ludwig, M. F. Schmalz, V. Knittel, D. Brida, and A. Leitenstorfer, "Sub-cycle optical phase control of nanotunnelling in the single-electron regime," Nat. Photonics **10**, 667–670 (2016).
23. M. Ludwig, G. Aguirregabiria, F. Ritzkowsky, T. Rybka, D. C. Marinica, J. Aizpurua, A. G. Borisov, A. Leitenstorfer, and D. Brida, "Sub-femtosecond electron transport in a nanoscale gap," Nat. Phys. **16**, 341–345 (2020).
24. T. Higuchi, C. Heide, K. Ullmann, H. B. Weber, and P. Hommelhoff, "Light-field-driven currents in graphene," Nature **550**, 224–228 (2017).
25. M. Schultze, E. M. Bothschafter, A. Sommer, S. Holzner, W. Schweinberger, M. Fiess, M. Hofstetter, R. Kienberger, V. Apalkov, V.

S. Yakovlev, M. I. Stockman, and F. Krausz, "Controlling dielectrics with the electric field of light," Nature **493**, 75–78 (2013).
26. A. Schiffrin, T. Paasch-Colberg, N. Karpowicz, V. Apalkov, D. Gerster, S. Mühlbrandt, M. Korbman, J. Reichert, M. Schultze, S. Holzner, J. V. Barth, R. Kienberger, R. Ernstorfer, V. S. Yakovlev, M. I. Stockman, and F. Krausz, "Optical-field-induced current in dielectrics," Nature **493**, 70–74 (2013).
27. P. Storz, J. Tauch, M. Wunram, A. Leitenstorfer, and D. Brida, "Parametric amplification of phase-locked few-cycle pulses and ultraviolet harmonics generation in solids at high repetition rate," Laser Photon. Rev. **11**, 1700062 (2017).
28. D. M. B. Lesko, H. Timmers, S. Xing, A. Kowligy, A. J. Lind, and S. A. Diddams, "A six-octave optical frequency comb from a scalable few-cycle erbium fibre laser," Nat. Photonics **15**, 281–286 (2021).
29. R. Hollinger, D. Hoff, P. Wustelt, *et al.*, "Carrier-envelope-phase measurement of few-cycle mid-infrared laser pulses using high harmonic generation in ZnO," Opt. Express **28**, 7314–7322 (2020).
30. R. Hollinger, P. Herrmann, V. Korolev, M. Zapf, V. Shumakova, R. Röder, I. Uschmann, A. Pugžlys, A. Baltuška, M. Zürch, C. Ronning, C. Spielmann, and D. Kartashov, "Polarization dependent excitation and high harmonic generation from intense mid-IR laser pulses in ZnO," Nanomaterials **11**, 4 (2021).
31. Z. Wang, H. Park, Y. H. Lai, J. Xu, C. I. Blaga, F. Yang, P. Agostini, and L. F. DiMauro, "The roles of photo-carrier doping and driving wavelength in high harmonic generation from a semiconductor," Nat. Commun. **8**, 1686 (2017).
32. X. Liu, X. Zhu, X. Zhang, D. Wang, P. Lan, and P. Lu, "Wavelength scaling of the cutoff energy in the solid high harmonic generation," Opt. Express **25**, 29216–29224 (2017).
33. S. Ghimire, A. D. DiChiara, E. Sistrunk, P. Agostini, L. F. DiMauro, and D. A. Reis, "Observation of high-order harmonic generation in a bulk crystal," Nat. Phys. **7**, 138–141 (2011).
34. S. Jiang, S. Gholam-Mirzaei, E. Crites, J. E. Beetar, M. Singh, R. Lu, M. Chini, and C. D. Lin, "Crystal symmetry and polarization of high-order harmonics in ZnO," J. Phys. B **52**, 225601 (2019).
35. G. Vampa, T. J. Hammond, N. Thiré, B. E. Schmidt, F. Légaré, C. R. McDonald, T. Brabec, and P. B. Corkum, "Linking high harmonics from gases and solids," Nature **522**, 462–464 (2015).
36. H. Timmers, M. Sabbar, J. Hellwagner, Y. Kobayashi, D. M. Neumark, and S. R. Leone, "Polarization-assisted amplitude gating as a route to tunable, high-contrast attosecond pulses," Optica **3**, 707–710 (2016).
37. T. J. Fellers and M. W. Davidson, "Concepts in digital imaging technology: CCD noise sources and signal-to-noise ratio," Hamamatsu/Florida State University, https://hamamatsu.magnet.fsu.edu/articles/ccdsnr.html, accessed 7 June 2022.
38. Y. S. You, Y. Yin, Y. Wu, A. Chew, X. Ren, F. Zhuang, S. Gholam-Mirzaei, M. Chini, Z. Chang, and S. Ghimire, "High-harmonic generation in amorphous solids," Nat. Commun. **8**, 724 (2017).
39. C. Benko, T. K. Allison, A. Cingöz, L. Hua, F. Labaye, D. C. Yost, and J. Ye, "Extreme ultraviolet radiation with coherence time greater than 1 s," Nat. Photonics **8**, 530–536 (2014).
40. H. Kato, M. Sano, K. Miyamoto, and T. Yao, "High-quality ZnO epilayers grown on Zn-face ZnO substrates by plasma-assisted molecular beam epitaxy," J. Cryst. Growth **265**, 375–381 (2004).
41. V. Schuster, C. Liu, R. Klas, P. Dominguez, J. Rothhardt, J. Limpert, and B. Bernhardt, "Ultraviolet dual comb spectroscopy: a roadmap," Opt. Express **29**, 21859–21875 (2021).
42. S. Galtier, C. Pivard, and P. Rairoux, "Towards DCS in the UV spectral range for remote sensing of atmospheric trace gases," Remote Sens. **12**, 3444 (2020).